PHYSICAL REVIEW B **96**, 024451 (2017)

Piezomagnetism as a counterpart of the magnetovolume effect in magnetically frustrated Mn-based antiperovskite nitrides

J. Zemen,[1,2,*] Z. Gercsi,[1,3] and K. G. Sandeman[1,4,5]
[1]*Department of Physics, Blackett Laboratory, Imperial College London, London SW7 2AZ, United Kingdom*
[2]*Faculty of Electrical Engineering, Czech Technical University in Prague, Technická 2, Prague 166 27, Czech Republic*
[3]*CRANN and School of Physics, Trinity College Dublin, Dublin 2, Ireland*
[4]*Department of Physics, Brooklyn College, CUNY, 2900 Bedford Ave., Brooklyn, New York 11210, USA*
[5]*Physics Program, The Graduate Center, CUNY, 365 Fifth Avenue, New York, New York 10016, USA*

(Received 30 December 2016; revised manuscript received 6 June 2017; published 31 July 2017)

Electric-field control of magnetization promises to substantially enhance the energy efficiency of device applications ranging from data storage to solid-state cooling. However, the intrinsic linear magnetoelectric effect is typically small in bulk materials. In thin films, electric-field tuning of spin-orbit-interaction phenomena (e.g., magnetocrystalline anisotropy) has been reported to achieve a partial control of the magnetic state. Here we explore the piezomagnetic effect (PME), driven by frustrated exchange interactions, which can induce a net magnetization in an antiferromagnet and reverse its direction via elastic strain generated piezoelectrically. Our *ab initio* study of PME in Mn-based antiperovskite nitrides identified an extraordinarily large PME in Mn_3SnN available at room temperature. We explain the magnitude of PME based on features of the electronic structure and show an inverse proportionality between the simulated zero-temperature PME and the magnetovolume effect at the magnetic (Néel) transition measured by Takenaka *et al.* in nine antiferromagnetic Mn_3AN systems.

DOI: 10.1103/PhysRevB.96.024451

I. INTRODUCTION

Emerging nonvolatile magnetic random access memory (MRAM) devices represent bits of information as a magnetization direction which needs to be stabilized by magnetic anisotropy. A spin-transfer torque (STT) is typically used to overcome the energy barrier between two stable directions. STT is induced by passing spin-polarized current which leads to Joule heating and sets limits on the storage density. Much research is focused on alternative switching mechanisms based on direct or indirect electric-field control of magnetic anisotropy which can reduce the dissipated energy by a factor of 100 [1]. At the same time antiferromagnetic (AFM) spintronics [2] explores alternatives to STT-MRAM devices based on active AFM components with a bistable alignment of the local magnetic moments. The switching then utilizes a spin-orbit torque (SOT) induced by an unpolarized electrical current in collinear AFMs [3,4] or STT due to a spin-polarized current in proposed noncollinear AFM junctions [5]. There is no dipolar coupling between neighboring elements and they are insensitive to external magnetic fields. Again this alternative promises a higher storage density and energy efficiency.

Here we explore the underlying physics required to postulate an ambitious approach combining the electric-field control of magnetic moments with the noncollinear antiferromagnetic structure of Mn-based antiperovskite nitrides. The required coupling between the spin and orbital degrees of freedom is dominated by geometrically frustrated exchange interactions. The indirect magnetoelectric effect (ME) is hosted by a piezomagnetic Mn-based antiperovskite layer elastically coupled to a piezoelectric substrate. We focus on the piezomagnetic effect (PME) which is characterized by a net magnetization that is directly proportional to the applied lattice strain [6,7]. Fully compensated AFM states are hard to track and utilize in general but the PME offers a valuable technique to probe and control the AFM ordering via the strain-induced magnetic moment.

To substantiate the future use of the PME in magnetoelectric composites, we perform a systematic *ab initio* study of PME in nine cubic antiperovskites Mn_3AN (A = Rh, Pd, Ag, Co, Ni, Zn, Ga, In, Sn). We explain the variation of the magnitude of PME across this range of compounds based on features of their electronic structure. The PME in Mn_3SnN predicted here is an order of magnitude larger than the PME modelled so far in Mn_3GaN [7]. Moreover, we compare the simulated PME to the measured magnetovolume effect (MVE) at a magnetic (Néel) transition temperature [8] across the full set of nine systems and shown that the effects are inversely proportional to each other. This agreement with experimental data is remarkable because both the PME and MVE originate in the frustrated AFM structure but we simulate the PME at zero temperature whereas the MVE was measured at the magnetic (Néel) transition temperature. The MVE has not been modelled for this set of systems before.

Note that Mn_3AgN and Mn_3RhN do not share the triangular AFM order according to earlier neutron-diffraction studies [9], whereas the magnetic structure of Mn_3CoN and Mn_3PdN is yet to be confirmed experimentally. We include these four compounds in our study as their composition, AFM order, and experimentally resolved MVE [8] makes them potential candidates for piezomagnetic behavior.

In more general terms, we perform a computational experiment when the magnetic system is initialized in the triangular state (representation Γ^{4g} or Γ^{5g} as described below) even if it was only a local energy minimum for Mn_3AN (A = Ag, Co, Pd, Rh) and the response (induced magnetization) to

---

[*] j.zemen@imperial.ac.uk

a tetragonal distortion is detected. The consistency of the piezomagnetic response across the whole set of materials motivates us to use this procedure as a probe of the level of frustration of the exchange interaction even if the real systems do not host piezomagnetism.

A. Mn-based antiperovskites

Mn-based antiperovskite nitrides were first examined in the 1970s [10,11]. More recent experimental work on these metallic compounds includes a demonstration of large negative thermal expansion (NTE) in Mn$_3$*A*N (A = Ga, Zn, Cu, Ni) [12–15] at the first-order phase transition to a PM state. A large barocaloric effect was measured in Mn$_3$GaN at $T_N = 288$ K [16] and the Mn-based antiperovskites were consequently proposed as a new class of mechanocaloric materials. More importantly for spintronic applications, the baromagnetic effect (BME), which is closely related to the PME, was reported in Mn$_3$G$_{0.95}$N$_{0.94}$ very recently [17], the exchange bias effect was observed in Mn$_3$GaN/Co$_3$FeN bilayers [18], perpendicular magnetic anisotropy was demonstrated in Mn$_{67}$Ga$_{24}$N on MgO substrate, and the magnetocapacitance effect was measured in Mn$_3$GaN/SrTiO$_3$ bilayers [19].

Theoretical work on Mn-based antiperovskites includes an early tight-binding study [20] suggesting that the proximity of the Fermi energy to a sharp singularity (narrow N$_p$-Mn$_d$ band) in the electronic density of states has a large influence on the stability of the structural and magnetic phases. However, this model considers only nearest-neighbor Mn-N hopping and neglects any hybridization with atom A. Phenomenological studies analyzed phase transitions [21], magnetoelastic, and piezomagnetic [6] properties with respect to the symmetry of the crystal and magnetic structure. More recently *ab initio* modeling of the noncollinear magnetic structure has been carried out. The NTE and MVE are attributed to the frustrated exchange coupling between the three Mn atoms [14,22,23]. The local spin density has been simulated for Mn$_3$GaN and Mn$_3$ZnN revealing its distinctly nonuniform distribution and localized character of the 3d Mn moment [24]. The piezomagnetic [7] and flexomagnetic effect [25] were simulated in Mn$_3$GaN by the same group. The strain-induced net magnetic moment predicted for Mn$_3$GaN is an order of magnitude lower than that of Mn$_3$SnN predicted in this work.

B. The piezomagnetic effect

The PME is defined by a linear dependence of the net magnetization on elastic stress tensor components, in contrast to the magnetoelastic effect where the dependence on stress is quadratic. Both effects can be described phenomenologically by adding appropriate stress-dependent terms to the free energy:

$$F(T,\boldsymbol{H},\sigma) = F_0(T,\boldsymbol{H}) - \lambda_{i,jk}H_i\sigma_{jk} - \mu_{i,jk}H_i\sigma_{jk}^2, \tag{1}$$

where $\lambda_{i,jk}$ is an axial time-antisymmetric tensor representing the PME, H_i are components of the magnetic field, σ_{jk} is the elastic stress tensor, and $\mu_{i,jk}$ is the magnetoelastic tensor. Nonvanishing elements of $\lambda_{i,jk}$ correspond to terms of Eq. (1) which are invariant under operations from the magnetic symmetry group [26]. These elements then contribute to the magnetization:

$$M_i = -\frac{\partial F}{\partial H_i} = -\frac{\partial F_0}{\partial H_i} + \lambda_{i,jk}\sigma_{jk} + \mu_{i,jk}\sigma_{jk}^2. \tag{2}$$

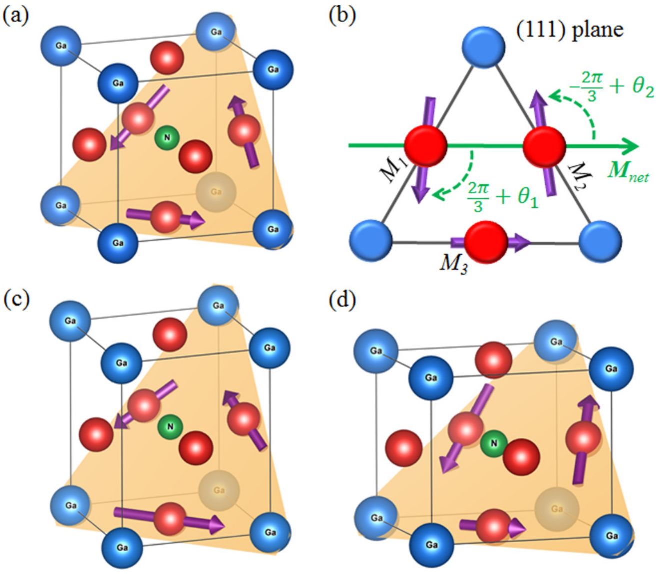

FIG. 1. Mn-based antiperovskite magnetic unit cell, cubic and strained lattice assuming Poisson's ratio of 0.5; the canting and changes of size are not to scale. (a) Unstrained structure of Mn$_3$GaN with local moments on Mn sites according to Γ^{5g} representation. (b) Tensile strained magnetic order in (111) plane; M_{net} indicates the direction of the induced net moment. (c) Compressively strained unit cell; (d) Tensile strained unit cell.

The PME was first proposed by Voigt [27] in 1928. The linear character limits its existence to systems without time-inversion symmetry or with a magnetic group that contains time inversion only in combination with other elements of symmetry [28]. Hence, the PME is forbidden in all paramagnetic and diamagnetic materials. The most striking manifestation of the PME is in antiferromagnets where the zero spontaneous magnetization acquires a finite value upon application of strain. The first AFM systems where PME was proposed [29,30] and later observed [31] were transition-metal difluorides. In Mn-based antiperovskite nitrides PME was predicted quantitatively in 2008 [7] and it has not been observed experimentally so far.

The noncollinear magnetic structure of Mn$_3$*A*N which hosts the PME and NTE considered in this work is shown in Fig. 1. (The direction of canting of the Mn local moments is specific for Mn$_3$GaN.) The ground state presented in Fig. 1(a) is the fully compensated AFM structure with symmetry corresponding to the Γ^{5g} representation [32]. (The magnetic unit cell belongs to the trigonal space group $P\bar{3}1m$ and has the same size as the cubic paramagnetic unit cell belonging to space group $Pm\bar{3}m$.) The exchange coupling between the neighboring Mn atoms is antiferromagnetic, which leads to the frustration in the kagome-type lattice in the (111) plane (highlighted as orange online). The three Mn local magnetic moments (LMMs) are of the same size and have an angle of $2\pi/3$ between their directions. Spin-orbit interaction (SOI) aligns the plane defined by the directions of the three

TABLE I. Physical properties of Mn_3AN: Néel temperature, lattice parameter at 10 K, calculated lattice parameter, spontaneous volume change, Poisson's ratio, bulk modulus, size of Mn local moment in unstrained system. All measured data are taken from Ref. [8] except a_0 and T_N for Mn_3SnN, which are from Ref. [9]. Calculated data are marked^t.

A	T_N [K]	a_0 [Å]	a_0^t [Å]	ω_s [10^{-3}]	ν^t	K^t [GPa]	M_0^t [μ_B]
Rh	226	3.918	3.88	2.07	0.19	148.4	2.84
Pd	316	3.982	3.94	3.60	0.20	140.7	3.15
Ag	276	4.013	3.98	5.79	0.20	118.9	3.08
Co	252	3.867	3.80	5.64	0.13	149.5	2.48
Ni	256	3.886	3.84	8.18	0.15	136.5	2.83
Zn	170	3.890	3.87	20.44	0.13	126.0	2.64
Ga	288	3.898	3.86	19.10	0.13	129.4	2.43
In	366	4.000	3.99	9.24	0.18	115.0	2.70
Sn	475	4.060	3.97	0.0	0.18	102.0	2.52

LMMs with the (111) lattice plane resulting in the Γ^{5g} representation of Fig. 1. A simultaneous rotation of all three LMMs by $\pi/2$ within the (111) plane results in another fully compensated AFM structure corresponding to the Γ^{4g} representation where the LMMs all point inside (outside) the triangle in a given (adjacent) plane [10]. The energy difference between Γ^{4g} and Γ^{5g} ordering is also purely due to SOI whereas the noncollinearity and the strong magneto-structural coupling is due to the exchange interaction. Note that the exchange interaction origin of the PME distinguishes it from magnetostriction, which is due to SOI [7]. The PME can be described as linear exchange-striction as the strength of the exchange interactions driving the PME is of the order of 10 meV per unit cell whereas the spin-orbit coupling falls between 0.1 and 1 meV per unit cell according to our *ab initio* simulations.

II. RESULTS

We calculate the total energy, magnetic moments, and projected density of states (DOS) for the noncollinear magnetic structure of biaxially strained Mn_3AN (A = Rh, Pd, Ag, Co, Ni, Zn, Ga, In, Sn) from first principles. Our computational procedure is the following:

(1) We find the equilibrium lattice parameter a_0, bulk modulus K, and Poisson's ratio ν for each material with fixed AFM order by fitting the total energies obtained for a range of lattice parameters (a,c/a) to the Birch–Murnaghan equation of state [33]. We also allowed for relaxation of individual atomic positions but we found no bond buckling in agreement with an earlier *ab initio* study [7]. The results are summarized in Table I.

(2) We relax the magnetic moments with a fixed lattice for a range of biaxial strains to evaluate the PME. We perform two independent sets of calculations with the vertical lattice parameter c set (a) to conserve the unstrained unit cell volume - data labeled "V", and (b) according to the calculated Poisson's ratio - data labeled "P". The initial AFM local moment directions and sizes are either relaxed by using a noncollinear implementation of spin-density functional theory (VASP code [34]) in a self-consistent loop or explicitly by searching for minima in a total energy profile $E_{\rm tot}(\varepsilon,\theta_1)$ as shown in Fig. 2. The quantitative agreement of these two methods gives us confidence that we have found the physically relevant energy minimum. All calculations include spin-orbit coupling and confirm that its impact on the PME is negligible in the case of period four and five elements.

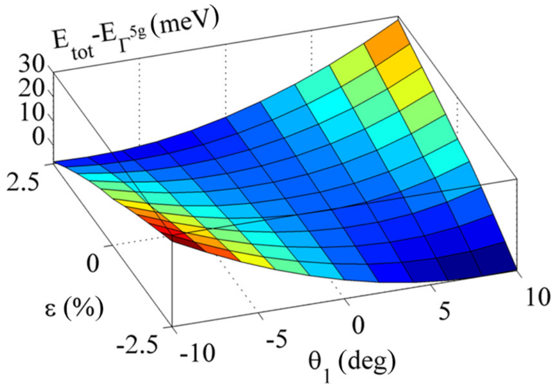

FIG. 2. Total energy as a function of biaxial strain and canted angle for Mn_3GaN. No interpolation is used in the surface plot. The equilibrium angle depends linearly on the strain. The reference energy corresponds to $E(\theta_1 = 0)$ for each strain.

(3) Finally, we increase the density of k-points and calculate the projected DOS for the converged strained and unstrained noncollinear structures to identify features in the electronic structure that would explain the variation of the PME across the material range. Our results do not confirm a proximity of the Fermi energy to a sharp peak in the DOS as suggested by an earlier tight-binding study [20].

Figures 1(c) and 1(d) represent a qualitative overview of the simulated response of the magnetic structure to the compressive and tensile strain, respectively. A comparison with the ground state in Fig. 1(a) shows that Mn magnetic moments cant and change size, which are two independent contributions to the PME. This behavior is due to the strain-induced reduction of symmetry from $P\bar{3}1m$ to the $Pm'm'm$ orthorhombic magnetic space group [7] and from $Pm\bar{3}m$ to the $P4/mmm$ tetragonal space group in the paramagnetic case [13] [the system is no longer invariant under the third-order rotation about the (111) axis].

For more clarity, Fig. 1(b) shows the tensile strained ($\varepsilon = \Delta a/a_0 > 0$) magnetic order in the (111) plane. The canted angles θ_i within the (111) plane and LMM magnitudes M_i on the three Mn sites are introduced. The moments in the (100) and (010) planes cant in opposite directions, $\theta_1 = -\theta_2$, to become more parallel (antiparallel) in case of positive (negative) θ_1. The moment in the (001) plane does not change direction.

The change of moment size $\Delta M_i = M_i - M_0$ is strongly dependent on the c/a ratio of the tetragonal lattice. (M_0 is the LMM size common to all Mn sites in the unstrained system.) The changes plotted in Fig. 1(b) correspond to unit-cell volume conservation when $\Delta M_1 = \Delta M_2 \approx -\Delta M_3/2$ for all systems studied. M_3 universally increases (decreases) with compressive (tensile) strain. With realistic Poisson's ratios all three Mn moments increase (decrease) for tensile (compressive) strain following the volume change of the unit

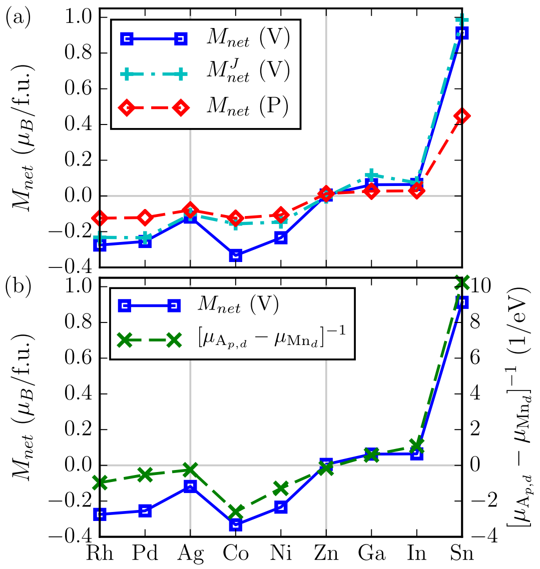

FIG. 3. Comparison of the net moment $M_{\rm net}$ induced by 1% of tensile strain: (a) $M_{\rm net}$ assuming unit-cell volume conservation (V) and Poisson ratios of Table I (P) and $M^J_{\rm net}$ fit according to Eq. (5). (b) Comparison of the PME, measured by $M_{\rm net}$(V), to the inverse of the energy separation between p or d states of atom A and d states of Mn, marked by the dashed line.

cell. (Mn_3RhN is the only exception where M_3 is almost independent of strain.) Atom A develops a moment two orders of magnitude lower than the Mn local moment for small applied strain, $|\varepsilon| < 1\%$, so its role in PME is negligible.

The unstrained ground state (plotted Γ^{5g}) has no spontaneous magnetization but a net moment $M_{\rm net}$ aligned with M_3 develops upon straining. Our calculations confirm that the canted angle θ_i, the change of moment size ΔM_i, and consequently $M_{\rm net} = 2M_1\cos(2\pi/3+\theta_1) + M_3$ depend linearly on applied strain as required by Eq. (2). The dependence departs slightly from linearity for larger strain $|\varepsilon| > 1\%$, and our study is limited to the interval $\varepsilon \in \langle -2.5, 2.5\rangle\%$. A striking feature of the PME is the change of orientation of $M_{\rm net}$ when switching between tensile and compressive biaxial strain. We note that such control of net moment orientation cannot be achieved by magnetostriction. [The same description holds also for Γ^{4g} order but $M_{\rm net} \parallel M_3$ is then rotated by $\pi/2$ in the (111) plane.]

Table I lists all relevant measured properties and results calculated in this work. Our Mn magnetic moment for Mn_3GaN is in good agreement with a previous theoretical study [7]. Our Poisson's ratios do not vary much across the range of compounds and are slightly smaller than $\nu = 0.25$–0.3 predicted by an *ab initio* study of elastic properties in $Mn_3(Cu,Ge)N$ [35]. All calculated lattice parameters are 1%–2% smaller than the values measured at low temperatures.

Figure 3 presents our results on the PME and the related features of electronic band structure. The net moment $M_{\rm net}$ plotted for the nine Mn-based antiperovskite systems subject to tensile strain $\varepsilon = 1\%$ is a natural measure of the PME. A positive (negative) value of $M_{\rm net}$ corresponds to a net moment induced parallel (antiparallel) to M_3 irrespective of belonging to the Γ^{4g} or Γ^{5g} representation.

Figure 3(a) compares the PME obtained assuming unit-cell volume conservation (Poisson's ratio $\nu = 0.5$) and using our calculated Poisson ratios ν listed in Table I, which correspond to smaller vertical distortion for a given strain. The latter is our lower estimate of the experimentally accessible PME as our calculated values of ν are lower than expected for metallic materials. The former version of the PME neglects the elastic properties of the lattice and represents the response of the frustrated magnetic system to a lattice symmetry breaking (normalized tetragonal distortion). As a result, the predicted $M_{\rm net}$ (V) should be regarded as an upper estimate of the experimentally accessible PME. In both cases Mn_3SnN is predicted to have $M_{\rm net}$ an order of magnitude larger than Mn_3GaN, the only PME value available in the literature [7].

A. Fitting the piezomagnetic effect with a Heisenberg model

To interpret the calculated PME in terms of the AFM pairwise exchange interactions $J_{ij}(\varepsilon)$ between the three Mn atoms in the (111) plane we resort to the classical Heisenberg model with variable moment sizes:

$$\begin{aligned} E(\theta_1,\varepsilon) = {} & -J_{12}M_1M_2\cos(2\pi/3-2\theta_1) \\ & -2J_{13}M_1M_3\cos(2\pi/3+\theta_1), \end{aligned} \tag{3}$$

where the values of the exchange parameters $J_{13} = J_{23} \neq J_{12}$ and the local moments $M_1 = M_2 \neq M_3$ introduced in Fig. 1(b) are restricted by the tetragonal symmetry of the lattice. We find the canted angle by minimizing the exchange energy ($\partial E/\partial\theta_1 = 0$) and insert it into the expression for the net moment $M_{\rm net} = 2M_1\cos(2\pi/3+\theta_1) + M_3$. We obtain a relationship between PME and changes of the exchange interaction due to strain:

$$\begin{aligned} \frac{M^{J'}_{\rm net}}{M_3} & \equiv 1 - \frac{J_{13}}{J_{12}} \\ & \approx \frac{J_0 - \Delta J - (J_0 + \Delta J)}{J_0 - \Delta J} \approx -\frac{2\Delta J}{J_0}, \end{aligned} \tag{4}$$

$$M^J_{\rm net} \equiv -\frac{2M_3}{J_0}\Delta J = \frac{2M_3}{J_0}\frac{\partial J_{12}}{\partial\varepsilon}\Delta\varepsilon, \tag{5}$$

where $M^{J'}_{\rm net}$ is an approximation of $M_{\rm net}$ based on our minimal model of Eq. (3), $J_0 < 0$ is the exchange parameter in the unstrained lattice, and ΔJ is the induced change of J_{12} and J_{13}. We have fit our *ab initio* total energy as a function of the canted angle to the Heisenberg model of Eq. (3) to extract J_{12} and J_{13} for each value of strain. In all compounds we have observed $J_{12} \approx J_0 - \Delta J$ and $J_{13} \approx J_0 + \Delta J$, which allows us to define $M^J_{\rm net}$ in Eq. (5) that is directly proportional to the derivative of the exchange parameters J_{ij} with respect to the biaxial strain ε.

Figure 3(a) shows that $M^J_{\rm net}$ is in good agreement with $M_{\rm net}$ (V) extracted directly from our calculated LMMs (without any fitting). The small differences are due to deviations of the magnetic system from Heisenberg behavior (e.g., LMMs change size as they cant even in an unstrained lattice) and deviations from linearity assumed in Eq. (4). The key conclusion based on Fig. 3(a) in combination with Eq. (4) is that a large PME corresponds to a large difference between J_{12}

(the bond in the plane of the biaxial strain) and J_{13} (the bond with a component perpendicular to this plane.)

We note that including exchange interactions to second-nearest neighbors in Eq. (3) would make sense only if the magnetic unit cell used in the *ab initio* calculation was increased beyond the chemical unit cell. However, so far there has not been sufficient experimental support for such an extension of our model.

B. Linking the piezomagnetic effect to band structure

Figure 3(b) relates the total induced moment M_{net} (V) to the mean band energy of the valence p or d states of atom A. This quantity is often called the band center and we extract it from our projected DOS, $\rho_{A_{p,d}}(E)$, as follows: $\mu_{A_{p,d}} = 1/\Omega \int E\rho_{A_{p,d}}(E)dE$, where $\Omega = \int \rho_{A_{p,d}}(E)dE$ is a normalization. We consider only the d band $[\rho_{A_d}(E)]$ when atom A is a transition metal and only the p band $[\rho_{A_p}(E)]$ for the rest. The wide s band does not seem to play an important role in the PME. The right vertical axis of Fig. 3(b) measures the inverse of $\mu_{A_{p,d}}$ with respect to the Mn d-band center, μ_{Mn_d}, which is very close to the Fermi energy.

Based on the remarkable match between $|M_{\text{net}}|$ and $(\mu_{A_{p,d}} - \mu_{Mn_d})^{-1}$ we conclude that piezomagnetism in Mn-based antiperovskite nitrides is governed by the mutual configuration of Mn d states and p or d states of atom A. More specifically, a greater proximity (a potential for hybridization) of the valence band of atom A to the spin-polarized d band of Mn increases the difference between J_{12} and J_{13} per unit strain, which manifests itself as a larger induced net moment. On the other hand, when the triangular magnetic order of Mn moments is undisturbed by hybridization with p or d states of atom A then $J_{12} \approx J_{13}$ and only a small net moment is induced. The best example is Mn_3ZnN where the narrow, fully filled d band is about 7 eV below the Fermi energy and the induced net moment is negligible. This trend is analogous to a scaling of the Néel temperature with the number of valence electrons of atom A, which was detected in 1977 in the same class of materials [11]. We further investigate the dependence of the sign of M_{net} on the presence of valence d states of atom A in a separate paper [36]. In the following paragraphs, we compare our simulated PME to the spontaneous MVE, which is another measure of the magnetic frustration and for which experimental data are available for all nine Mn_3AN compounds [8].

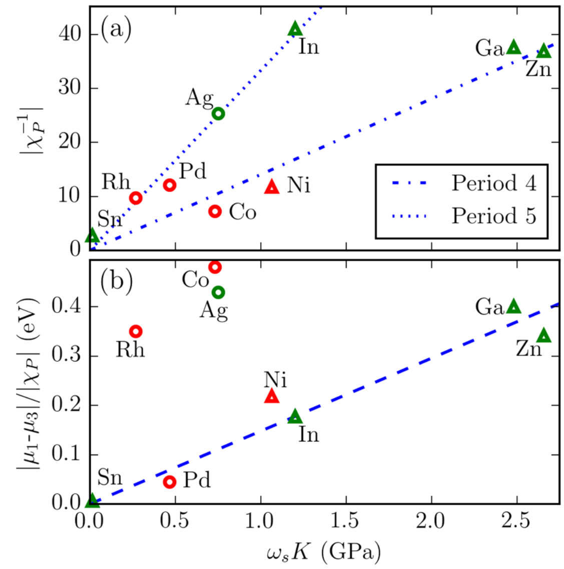

FIG. 4. Calculated PME characterized by $|\chi_P^{-1}|$ as a function of the measured MVE weighted by the bulk modulus. Triangles indicate systems with confirmed triangular magnetic ground state, red and green symbols indicate a positive and negative canted angle at tensile strain, respectively, and the blue lines are least square linear fits. (a) Two different trends for atom A from period four and five; (b) $|\chi_P^{-1}|$ weighted by a strain-induced shift of mean band energy of two Mn atoms: one trend for all systems with confirmed triangular magnetism.

C. Comparing the piezomagnetic effect to the magnetovolume effect

To draw an analogy between the strain and an external field H that can induce magnetization, we introduce a piezomagnetic susceptibility:

$$\frac{M_{\text{net}}^J}{M_3} = \frac{2}{J_0}\frac{\partial J_{12}}{\partial \varepsilon}\Delta\varepsilon \equiv \chi_P(\mu_{A_{p,d}})\Delta\varepsilon, \tag{6}$$

where the change of applied strain $\Delta\varepsilon$ replaces H and $M_{\text{net}}^J(\Delta\varepsilon)$ was introduced in Eq. (5). Based on Fig. 3(b) we can say that the susceptibility $\chi_P(\mu_{A_{p,d}})$ is inversely proportional to the mean valence-band energy of atom A (with respect to the Mn d-band center μ_{Mn_d}) in the unstrained system.

Figure 4 compares the measured magnetovolume effect [8] to our calculated piezomagnetic susceptibility χ_P. The MVE is a spontaneous change of volume due to a change of magnetic ordering (typically the size of magnetic moment). It was first observed in Ni-Fe Invar below its T_C [37]. Takenaka *et al.* measure a spontaneous volume increase upon the transition from the PM to AFM state and subtract the phononic contribution so that their MVE data are purely of magnetic origin [8]. They investigate a wide range of Mn-based antiperovskite nitrides and conclude that the MVE is a property of the frustrated triangular AFM state, which is strongly dependent on the number of valence electrons. The MVE is the largest when there are two s electrons and one or no p electrons (A = Zn, Ga). When the number of valence s and p electrons changes then the system transforms to a different crystal and magnetic structure with no MVE (A = Cu, Ge, As, Sn, Sb).

In addition, Takenaka *et al.* have observed an increase in MVE as the d band of atom A moves away from E_F. This general trend reminds us of the scaling of susceptibility χ_P with the mean band energy of atom A, $\mu_{A_{p,d}}$, described above. We include Fig. 4(a) to check if the dependence on $\mu_{A_{p,d}}$ furnishes a clear link between the PME and MVE. The figure shows that our piezomagnetic susceptibility χ_P is inversely proportional to the measured volume change, as expected. In other words, a large MVE implies a small PME and vice versa. Atoms A belonging to periods four and five of the periodic table have different coefficients of proportionality. This implies that not only the position of the A band with respect to E_F but also the size of atom A plays a role in weakening the triangular AFM structure. Such a difference between periods four and five was first also seen by Fruchart and Bertaut in the case of the scaling of T_N with the number of valence electrons of atom A [11].

The agreement of a calculated zero-temperature susceptibility (χ_P^{-1}) with a spontaneous volume change ω_s at the PM-AFM phase transition (weighted by K) is remarkable and requires further analysis. Magnetovolume effects in itinerant electron magnets were first analyzed by the Stoner–Edwards–Wohlfarth theory [38]. The free energy can be approximated by $F(T,M,\omega) = F_0(T,\omega) + \frac{1}{2}KV\omega^2 + \frac{1}{2}a(T,\omega)M^2$ and minimized with respect to the volume strain $\omega = \Delta V/V$ to obtain $KV\omega = c_{mv}M^2$ where $c_{mv} = -\frac{1}{2}\partial a(T,\omega)/\partial\omega$ is the magnetovolume coefficient, M is the spontaneous magnetization, K is the bulk modulus, and V is the reference volume. After considering the spin fluctuations at the first-order phase transition, the above formula becomes $KV\omega = c_{mv}(M^2 - \xi^2)$, where ξ is the amplitude of spin fluctuations [39,40].

In the case of Mn-based antiperovskites the local moments are relatively well localized [24], so we can approximate the magnetic energy of the triangular AFM system on a cubic lattice by Eq. (3) with zero canted angle: $E(\theta_1 = 0) = \frac{3}{2}J_0M_0^2$. The balance of elastic and magnetic energy then leads to an expression for the spontaneous volume strain ($\Delta V/V$):

$$\omega_s K = -\frac{3M_0^2}{2V}\frac{\partial J_0}{\partial\omega} \sim \frac{\partial J_0}{\partial\omega} \equiv t^v, \tag{7}$$

where we neglect the change of local moments M_0 with changing volume, $(\Delta M_0)^2$, as a higher-order contribution. The magnetic stress per Mn-Mn bond t^v is introduced following the work of Filippetti and Hill [41]. The magnetic stress at the phase transition can then be expressed as $T^v = \partial E^{\Gamma^{5g}}/\partial\omega = \frac{3}{2}t_v M_0^2$, where $E^{\Gamma^{5g}}$ is again the magnetic energy $E(\theta_1 = 0)$.

After establishing the link between MVE and the magnetic volume stress T^v, we attempt the same for the PME and the magnetic biaxial stress: $T^b = \partial E(\theta_1)/\partial\varepsilon \sim t^b$, where $E(\theta_1)$ is a magnetic energy of the canted AFM structures and the magnetic stress per Mn-Mn bond t^b is proportional to the susceptibility χ_P of Eq. (6):

$$\chi_P = \frac{2}{J_0}\frac{\partial J_{12}}{\partial\varepsilon} \sim \frac{\partial J_{12}}{\partial\varepsilon} \equiv t^b. \tag{8}$$

Finally, based on the comparison of Eqs. (7) and (8) we can conclude that both $\omega_s K$ and χ_P are proportional to derivatives of the exchange parameters with respect to strain and thereby to the magnetic stress of the triangular AFM system. Hence the linear relationship of Fig. 4(a) indicates a trade-off between two complementary stress relief mechanisms.

III. DISCUSSION

In principle, the stress arising at the onset of AFM ordering at T_N can be relieved by a volume change or a lattice distortion. However, our calculations and subsequent fitting to the Heisenberg model find that the magnetic energy saved by a tetragonal distortion (linear in ε) becomes smaller than the elastic energy cost (quadratic in ε around unstrained lattice) for negligibly small distortions. This is confirmed by x-ray diffraction [8], which has not indicated a tetragonal distortion in any compound studied in this work. Nevertheless, χ_P reflects how much magnetic stress could be relieved by a tetragonal distortion and this quantity is inversely proportional to $\omega_s K$, as shown by Fig. 4. We plot χ_P vs $\omega_s K$ rather than ω_s to compare only quantities related to magnetism and factor out the system-dependent elastic properties.

It should be noted that the sign of χ_P indicates which type of tetragonal distortion is energetically more favorable. A brief demonstration of this neglects the dependence of M_i and θ_i on strain in Eq. (3). Then we can find a spontaneous biaxial strain ε_s (analogous to volume strain ω_s) from the balance of elastic and magnetic energy: $\varepsilon_s = \frac{1}{2C}\partial J_{12}/\partial\varepsilon M_0^2 = -\frac{1}{4C}\chi_P|J_0|M_0^2$, where $C > 0$ is an effective elastic modulus. Immediately, we can see that all systems in this study with $\chi_P > 0$ tend to a distortion with $\varepsilon_s < 0$ ($c/a > 1$) and vice versa.

We conclude that a system with robust triangular magnetic order undisturbed by the proximity of electronic states of atom A (large $\mu_{A_{p,d}}$) tends to relieve its magnetic stress via a volume change, whereas a system more influenced by atom A but with persisting triangular order (small $\mu_{A_{p,d}}$) prefers to relieve its magnetic stress via a tetragonal distortion should the elastic-energy cost allow it. (If the tetragonal distortion is enforced externally, then the system develops a large net magnetization.)

The slight deviations of $|\chi_P^{-1}|$ from $\omega_s K$ seen in Fig. 4 may originate in (a) spin fluctuations which we neglected in Eq. (7), the small size of the deviations suggests that the spin-fluctuation contribution to the MVE $[KV\omega = c_{mv}(M^2 - \xi^2)]$ is significantly suppressed by the strong frustration; (b) limited numerical accuracy, e.g., $\mathrm{Mn_3ZnN}$ is most affected because it has very small χ_P and its large relative error is amplified by the inversion; (c) nitrogen deficiency (8%–16%) varying across the range of samples where MVE was measured [8], e.g., magnetic order in $\mathrm{Mn_3SnN}$ is known to be sensitive to N concentration [9]; and (d) a material-specific elastic property that was not factored out of the plotted quantities, e.g., the use of bulk modulus $K = 130$ GPa for all compounds when subtracting the phononic contribution to the MVE [8] (consequently, in the plot we use $K = 130$ GPa instead of our calculated K of Table I).

To further explore the inverse proportionality between PME and MVE with respect to features of the electronic structure we analyze the strain dependence of the mean band energy of Mn states. We extract the mutual shift of mean band energy of Mn_d^1 states [site in (100) plane of the unit cell] and Mn_d^3 [site in (001) plane] from the projected DOS $\rho_{Mn_d^1}(E,\varepsilon,\theta_1)$ and $\rho_{Mn_d^3}(E,\varepsilon,\theta_1)$ of the strained system before canting ($\varepsilon = 1\%$, $\theta_1 = 0$) in analogy to evaluation of $\mu_{A_{p,d}}$ shown in Fig. 3(b). The obtained quantity $|\mu_1 - \mu_3|$ directly measures the response of the spin-polarized electronic structure to the tetragonal distortion. Such information is missing in $\mu_{A_{p,d}}$ of the unstrained structure.

Figure 4(b) shows $|\chi_P^{-1}|$ weighted by the mutual band shift $|\mu_1 - \mu_3|$ as a function of $\omega_s K$. Compounds with atom A from periods four and five now follow the same linear trend with the exception of $A =$ Ag, Co, Rh. Our hypothesis based on Fig. 4 is that the factor $|\mu_1 - \mu_3|$ incorporates the dependence of the PME on the size of atom A for systems with stable triangular AFM ordering. $\mathrm{Mn_3AgN}$ and $\mathrm{Mn_3RhN}$ do not have a triangular AFM ground state, which has an explanation in their band-structure properties and becomes apparent in Fig. 4(b). Extending the same argument to those compounds with unknown magnetic order, we expect Mn_3PdN (Mn_3CoN) to have a triangular (other) AFM ground state.

The linear scaling of the spontaneous MVE with $|\chi_P^{-1}|$ implies a significant suppression of spin fluctuations by the strong frustration in these systems. At the same time it can be used as a tool in theory-led design of nonstoichiometric materials with a large MVE and, consequently, barocaloric effect where the entropy change is proportional to the spontaneous volume change according to the Clausius–Clapeyron relation:

$$S(T_t,p) - S(T_t,0) = V\omega_s\left(\frac{dT_t}{dp}\right)^{-1}. \tag{9}$$

Modelling the pressure dependence of the transition temperature dT_t/dp goes beyond the capability of density functional theory at zero temperature and is the subject of our ongoing work [36].

In terms of practical devices hosting the composite magnetoelectric effect we envisage a piezomagnetic Mn-based antiperovskite layer grown on a piezoelectric substrate. Such a bilayer can benefit from strong elastic coupling due to the common perovskite structure with small lattice mismatch at the interface. In case of a multidomain state in the as-grown AFM layer one can apply biaxial strain that induces a net moment along an arbitrary direction in each domain. Then an external magnetic field (coupling to the induced moment in each domain) can align all domains and increase the net magnetization. This magnetization will persist when the external field is removed. After removing the biaxial strain the net magnetization will vanish but the antiferromagnetic domains will remain ordered due to the magnetocrystalline anisotropy of the order of 0.1–1 meV per unit cell.

We hope that the successful comparison of our predicted PME to the measured MVE and the coherent interpretation of the PME based on features of the electronic structure will provide guidance for further investigations of the unique physical properties of the frustrated AFM structure of Mn-based antiperovskites and enable development of applications including data storage, memory, and solid-state cooling.

IV. METHODS

All our calculations employ the projector augmented-wave (PAW) method implemented in VASP code [34] within the Perdew–Burke–Ernzerhof (PBE) generalized gradient approximation [42]. The relaxation of fully unconstrained noncollinear magnetic structures has been implemented by Hobbs [43]. The relativistic effects are accounted for by a Hamiltonian containing the mass-velocity and Darwin corrections and the spin-orbit operator $\mathbf{L}\cdot\mathbf{S}$ in a basis of total-angular-momentum eigenstates as implemented by Kresse and Lebacq [44]. The off-diagonal elements of the 2×2 matrix in spin space originate in spin-orbit coupling and also in the exchange-correlation potential in the case of noncollinear magnetization density.

We use a $12\times 12\times 12$ k-point sampling in the self-consistent cycle and $17\times 17\times 17$ k-point sampling to obtain the site and orbital-resolved DOS. The cutoff energy is 400 eV. The local magnetic moments are evaluated in atomic spheres with the default Wigner Seitz radius because they are not very sensitive to the projection sphere radius [7].

We constrain the Mn local moment directions by using an additional penalty energy as implemented in the VASP code in order to obtain the DOS projected on Mn d states, e.g., $\rho_{Mn_d^3}(E,\varepsilon,\theta_1)$ of the strained system. We add a further constraint to suppress the small moment on atom A which develops due to strain to allow for extraction of J_{12} and J_{13} from the total energy as a function of strain and canted angle by fitting to the Heisenberg model of Eq. (3).

ACKNOWLEDGMENTS

We would like to thank Kirill Belashchenko, Lesley Cohen, Julie Staunton, and Eduardo Mendive-Tapia for productive discussions. The research leading to these results has received funding from the European Union Seventh Framework Programme (FP7/2007- 2013) under Grant Agreement No. 310748 (DRREAM).

---

[1] F. Matsukura, Y. Tokura, and H. Ohno, Nat. Nanotechnol. **10**, 209 (2015).

[2] T. Jungwirth, X. Marti, P. Wadley, and J. Wunderlich, Nat. Nanotechnol. **11**, 231 (2016).

[3] P. Wadley, B. Howells, J. Železný, C. Andrews, V. Hills, R. P. Campion, V. Novak, K. Olejník, F. Maccherozzi, S. Dhesi *et al.*, Science **351**, 587 (2016).

[4] J. Železný, H. Gao, K. Výborný, J. Zemen, J. Mašek, A. Manchon, J. Wunderlich, J. Sinova, and T. Jungwirth, Phys. Rev. Lett. **113**, 157201 (2014).

[5] J. Zelezny, Y. Zhang, C. Felser, and B. Yan, arXiv:1702.00295.

[6] E. Gomonaj, Phase Transit. **18**, 93 (1989).

[7] P. Lukashev, R. F. Sabirianov, and K. Belashchenko, Phys. Rev. B **78**, 184414 (2008).

[8] K. Takenaka, M. Ichigo, T. Hamada, A. Ozawa, T. Shibayama, T. Inagaki, and K. Asano, Sci. Tech. Adv. Mater. **15**, 015009 (2014).

[9] Ph. L'Héritier, D. Fruchart, R. Madar, and R. Fruchart, 1.5.6.2 Crystallographic properties of $M_cXM_3^f$ compounds, in *Alloys and Compounds of d-Elements with Main Group Elements. Part 2*, edited by H. P. J. Wijn, Landolt-Börnstein - Group III Condensed Matter Vol. 19C (Springer-Verlag, Berlin, Heidelberg, 1988).

[10] D. Fruchart, E. Bertaut, R. Madar, G. Lorthioir, and R. Fruchart, Solid State Commun. **9**, 1793 (1971).

[11] D. Fruchart and F. Bertaut, J. Phys. Soc. Jpn. **44**, 781 (1978).

[12] K. Takenaka and H. Takagi, Appl. Phys. Lett. **87**, 261902 (2005).

[13] M. Wu, C. Wang, Y. Sun, L. Chu, J. Yan, D. Chen, Q. Huang, and J. W. Lynn, J. Appl. Phys. **114**, 123902 (2013).

[14] S. Deng, Y. Sun, H. Wu, Q. Huang, J. Yan, K. Shi, M. I. Malik, H. Lu, L. Wang, R. Huang *et al.*, Chem. Mater. **27**, 2495 (2015).

[15] S. Deng, Y. Sun, L. Wang, Z. Shi, H. Wu, Q. Huang, J. Yan, K. Shi, P. Hu, A. Zaoui *et al.*, J. Phys. Chem. C **119**, 24983 (2015).

[16] D. Matsunami, A. Fujita, K. Takenaka, and M. Kano, Nat. Mater. **14**, 73 (2015).

[17] K. Shi, Y. Sun, J. Yan, S. Deng, L. Wang, H. Wu, P. Hu, H. Lu, M. I. Malik, Q. Huang *et al.*, Adv. Mater. **28**, 3761 (2016).

[18] H. Sakakibara, H. Ando, Y. Kuroki, S. Kawai, K. Ueda, and H. Asano, J. Appl. Phys. **117**, 17D725 (2015).

[19] H. Tashiro, R. Suzuki, T. Miyawaki, K. Ueda, and H. Asano, J. Korean Phys. Soc. **63**, 299 (2013).

[20] J.-P. Jardin and J. Labbé, J. Appl. Phys. **52**, 1627 (1981).

[21] E. Gomonaj and V. L'vov, Phase Transit. **38**, 15 (1992).

[22] B. Y. Qu and B. C. Pan, J. Appl. Phys. **108**, 113920 (2010).

[23] B. Qu, H. He, and B. Pan, Adv. Condens. Matter Phys. **2012**, 7 (2012).

[24] P. Lukashev and R. F. Sabirianov, J. Appl. Phys. **107**, 09E115 (2010).

[25] P. Lukashev and R. F. Sabirianov, Phys. Rev. B **82**, 094417 (2010).

[26] A. Borovik-Romanov, Ferroelectrics **162**, 153 (1994).

[27] W. Voigt, *Lehrbuch der Kristallphysik* (Leipzig, 1928).

[28] B. A. Tavger and V. M. Zaitzev, J. Exp. Theor. Phys. (USSR) **3**, 430 (1956).

[29] I. E. Dzyaloshinskii, J. Exp. Theor. Phys. (USSR) **33**, 807 (1957).

[30] T. Moriya, J. Phys. Chem. Solids **11**, 73 (1959).

[31] A. Borovik-Romanov, J. Exp. Theor. Phys. (USSR) **36**, 1954 (1959); **38**, 1088 (1960).

[32] E. Bertaut, D. Fruchart, J. Bouchaud, and R. Fruchart, Solid State Commun. **6**, 251 (1968).

[33] F. Birch, Phys. Rev. **71**, 809 (1947).

[34] G. Kresse and D. Joubert, Phys. Rev. B **59**, 1758 (1999).

[35] B. Qu, H. He, and B. Pan, AIP Adv. **1**, 042125 (2011).

[36] J. Zemen, E. Mendive-Tapia, Z. Gercsi, R. Banerjee, J. B. Staunton, and K. G. Sandeman, Phys. Rev. B **95**, 184438 (2017).

[37] M. Hayase, M. Shiga, and Y. Nakamura, J. Phys. Soc. Jpn. **34**, 925 (1973).

[38] E. Wohlfarth, Physica B + C (Amsterdam) **91**, 305 (1977).

[39] T. Moriya and K. Usami, Solid State Commun. **34**, 95 (1980).

[40] Y. Takahashi and H. Nakano, J. Phys.: Condens. Matter **18**, 521 (2006).

[41] A. Filippetti and N. A. Hill, Phys. Rev. Lett. **85**, 5166 (2000).

[42] J. P. Perdew, K. Burke, and M. Ernzerhof, Phys. Rev. Lett. **77**, 3865 (1996).

[43] D. Hobbs, G. Kresse, and J. Hafner, Phys. Rev. B **62**, 11556 (2000).

[44] P. Błoński, S. Dennler, and J. Hafner, J. Chem. Phys. **134**, 034107 (2011).